
HAL-BASED PLUGIN ESTIMATION OF THE CAUSAL DOSE-RESPONSE CURVE

A PREPRINT

✉ **Junming (Seraphina) Shi**
Department of Biostatistics
University of California, Berkeley
Berkeley, CA 94704
junming_shi@berkeley.edu

✉ **Wenxin Zhang**
Department of Biostatistics
University of California, Berkeley
Berkeley, CA 94704
hubbard@berkeley.edu

✉ **Alan E. Hubbard**
Department of Biostatistics
University of California, Berkeley
Berkeley, CA 94704
hubbard@berkeley.edu

✉ **Mark J. van der Laan**
Department of Biostatistics
University of California, Berkeley
Berkeley, CA 94704
laan@berkeley.edu

November 21, 2024

ABSTRACT

Estimating the marginally adjusted dose-response curve for continuous treatments is a longstanding statistical challenge critical across multiple fields. In the context of parametric models, misspecification may result in substantial bias, hindering the accurate discernment of the true data generating distribution and the associated dose-response curve. In contrast, non-parametric models face difficulties as the dose-response curve isn't pathwise differentiable, and then there is no \sqrt{n} -consistent estimator. The emergence of the Highly Adaptive Lasso (HAL) MLE by van der Laan [2015] and van der Laan [2017] and the subsequent theoretical evidence by van der Laan [2023] regarding its pointwise asymptotic normality and uniform convergence rates, have highlighted the asymptotic efficacy of the HAL-based plug-in estimator for this intricate problem. This paper delves into the HAL-based plug-in estimators, including those with cross-validation and undersmoothing selectors, and introduces the undersmoothed smoothness-adaptive HAL-based plug-in estimator. We assess these estimators through extensive simulations, employing detailed evaluation metrics. Building upon the theoretical proofs in van der Laan [2023], our empirical findings underscore the asymptotic effectiveness of the undersmoothed smoothness-adaptive HAL-based plug-in estimator in estimating the marginally adjusted dose-response curve.

Keywords Dose-Response Curves · Counterfactual Interventions · Asymptotically Efficient Estimator · Causal Inference · Highly Adaptive Lasso · HAL MLE · Càdlàg Functions · Cross-Validation · Non-Pathwise Differentiable Parameter

1 Introduction

A marginally adjusted ("causal") dose–response curve, or a controlled direct effects curve, is a graphical representation of the causal relationship between a treatment or intervention and the outcome of interest, taking into account potential confounding factors and where the treatment or intervention is continuous or ordinal. Estimating the marginally adjusted dose–response is a common problem in causal inference and efficient estimators with valid inferences are crucial for a wide range of scientific applications, including epidemiology, medical research, social sciences, and many other fields. For example, in a clinical trial investigating the impact of a drug with continuous dosage on blood pressure reduction, estimating the marginally adjusted dose–response curve becomes crucial. This allows clinicians to identify the specific reduction or increase in blood pressure attributable to each incremental change in drug dosage while accounting for potential confounding factors such as age, gender, and baseline blood pressure. This precise insight is essential for optimizing treatment plans and ensuring both the efficacy and safety of the therapeutic intervention.

To estimate the causal dose–response curve and associated causal direct effects, we need to define a parameter $\mathbb{E}[Y_a]$ under the counterfactual or potential outcomes framework where what would be observed if, possibly contrary to the real world, all subjects in the target population would have received treatment with level a (van der Laan and Petersen [2008], Petersen et al. [2006], Rubin [2004]). This counterfactual is widely studied and commonly used in causal inferences to estimate the causal effects of binary interventions (Van der Laan et al. [2011], Rubin [2006], Laan and Robins [2003], Abadie and Imbens [2006], Angrist and Imbens [1995], Robins [1986], Rubin [1978]). Consistent and efficient estimators based on inverse probability of treatment weighting (IPTW) (Austin and Stuart [2015]), augmented IPTW (A-IPTW) (Luque-Fernandez et al. [2018]), targeted learning (TMLE) (Van der Laan et al. [2011]), or highly adaptive lasso (HAL) (van der Laan [2017]) and undersmoothed HAL (van der Laan et al. [2022]) have been developed to provide reliable inference for binary treatment effect. However, a large number of causal inference problems are inherently defined in terms of continuous nature and there are very few consistent and efficient estimators applied for the causal dose–response curve for continuous treatments. The reason is that the causal dose–response curve for continuous treatments in a nonparametric model is not pathwise differentiable (Bickel et al. [1993]). Consequently, root- n estimators are not applicable, leading to reliance on estimators that depend on data density rather than a smooth function of this density.

Considerable efforts have been dedicated to crafting estimators for the causal dose–response curve, highlighting the challenges faced when applying supervised models to minimize observed error in counterfactual inference tasks. The inherent bias in treatment assignments and the inability to observe counterfactual outcomes often render these models ineffective. The Marginal Structural Model (MSM) framework, initially introduced by Robins et al. [2000], is renowned for its capability to estimate causal dose–response curves. However, its efficacy is contingent upon the inclusion of the true dose–response curve within the model, alongside its structural causal assumptions. To mitigate issues of model misspecification, Neugebauer and van der Laan [2007] refined the MSM approach by projecting the true causal dose–response curve onto a functional space defined by MSM’s parameterization, aiming to enhance model robustness. Despite these advancements, there remains a keen interest in directly analyzing the actual curve, rather than its projection. This has prompted numerous studies, including works by Hirano and Imbens [2004], Callaway et al. [2021], Schwab et al. [2020] and Díaz and van der Laan [2013], to develop estimators employing non-parametric methods. Nonetheless, these methods grapple with challenges such as the curse of dimensionality, assumptions with limited applicability, or difficulties in yielding valid inferences. While the Cross-Validated Targeted Maximum Likelihood Estimation (CV-TMLE) by Van der Laan and Rose [2018] and the nonparametric causal inference method (npcausal) by Kennedy et al. [2017] achieve asymptotic normality, facilitating inference, they are constrained by their dependency on dimension and smoothness. Furthermore, their reliance on kernel smoothing introduces complexities in selecting the tuning parameter, particularly given the suboptimal performance of global cross-validation selectors for bandwidth selection at specific points.

In this article, we introduce and refine the HAL-based plugin estimator for marginally adjusted causal dose–response with augmentations for controlled direct effects curves. Highly Adaptive Lasso (HAL) MLE is a nonparametric minimum loss estimator that can create efficient estimators for pathwise differentiable parameters with theoretical proofs. Moreover, for non-pathwise differentiable parameters, the marginal dose–response curve in our case, rigorous theoretical evidence confirms that HAL-based plugin estimator is pointwise asymptotically normal and converges to the true curve at a dimension free rate up till $\log n$ factors (van der Laan [2023]). Our simulation study aims to assess the performance of estimators under various conditions and to show that the HAL-based plugin estimator is pointwise asymptotically normal, delivering satisfactory confidence intervals for estimating the causal dose–response curve.

We begin with an overview of the High Adaptive Lasso (HAL) MLE methodology, revisit the undersmoothing criteria in the context of HAL-MLE, and review the pointwise asymptotic normality. Following this foundation, we delineate our target parameter and introduce the HAL-based plug-in estimator with the delta-method based inference. Subsequently, through a series of simulation tests, we demonstrate that the HAL-based plugin estimator reliably

produces asymptotically normal results with a constant convergence rate and delta-method based confidence intervals of satisfactory coverage.

2 Method

2.1 Càdlàg functions with finite sectional variational norms

To comprehend the Highly Adaptive Lasso (HAL), it's pivotal to recognize its core: multivariate real-valued càdlàg functions with finite sectional variation norms (FSVN). These functions are highly flexible, being right-continuous with left limits and capable of including jumps and quadratic curves, without the strict need for smoothness.

The class of càdlàg functions with FSVN constitutes a Donsker class, ensuring that empirical processes indexed by this class converge to Gaussian processes, as established by empirical process theory. The Highly Adaptive Lasso (HAL) is obtained by minimizing empirical risk over this class of càdlàg functions. Since this class of functions represents a realistic model for the true target function and remains small enough to control the supremum norm of empirical processes, such minimum empirical risk estimators yield well-behaved estimators in terms of convergence rate and asymptotic normality. Consequently, the Highly Adaptive Lasso is a Maximum likelihood (or more generally, minimum empirical risk) estimator developed to leverage the advantages of this class of functions.

Let $Q : [0, 1]^d \rightarrow \mathbb{R}$ be a d -variate càdlàg function with on the unit cube. It can be represented as

$$\begin{aligned} Q(x) &= Q(0) + \sum_{S \subset \{1, \dots, d\}} \int_{(0(S), x(S))} Q_S(du) \\ &= Q(0) + \sum_{S \subset \{1, \dots, d\}} \int_{(0(S), x(S))} I(u \leq x(S)) Q_S(du), \end{aligned} \tag{1}$$

where for subset S of $\{1, \dots, d\}$, and x in $[0, 1]^d$, we define $x(S) = (x(j) : j \in S)$ and $Q_S(x(S)) = Q(x(S), 0(-S))$ as the S -specific section of Q that sets the coordinates outside S equal to zero.

Consequently, càdlàg functions can be approximated by a linear combination of zero-order splines $x \rightarrow I(u \leq x(s))$ indexed by a knot-point u , defined by a set of support points, and $dQ_{m,S,j}$ now simply represent coefficients in this linear model,

$$Q_m(x) = Q(0) + \sum_{S \subset \{1, \dots, d\}} \sum_j I(s_j(S) \leq x(S)) dQ_{m,S,j}. \tag{2}$$

This discrete approximation is a linear combination of basis functions $x \rightarrow \phi_{j,S}(x) = I(x(S) \geq s_j(S))$ with corresponding coefficients $dQ_{m,S,j}$ across $S \subset \{1, \dots, d\}$ and support points $s_j \in [0, 1]^d$, $j = 1, \dots, m$.

The sectional variational norm is the sum of the variation norms across all its sections. Mathematically, it's given by $\|Q\|_v^* = \int_{[0,1]^d} |dQ(x)|$, where dQ is the sum measure over the interior $(0, 1]^d$ and all zero edges. That is, $\|Q\|_v^* = |Q(0)| + \sum_{S \subset \{1, \dots, d\}} \int_{(0(S), 1(S))} |dQ_S(u)|$. The sectional variation norm of the discrete approximation is given by $\|Q_m\|_v^* = |Q(0)| + \sum_{S \subset \{1, \dots, d\}} \sum_j |dQ_{m,S,j}|$. So note that the latter sectional variation norm is just the L_1 -norm of the coefficients.

Assuming that the true function Q_0 falls in a class of càdlàg functions with bound M on sectional variation norm is a realistic assumption. This assumption renders this class suitable for realistic modeling of data distributions. Moreover, it facilitates dimension-free convergence rates, particularly up to $\log(n)$, further enhancing its theoretical attractiveness and practical utility.

2.2 Highly Adaptive Lasso (HAL)

2.2.1 Definition of HAL

The Highly Adaptive Lasso (HAL) is a nonparametric minimum loss estimator. In its most nonparametric form, HAL only assumes the estimated function belongs to the class of d -variate real-valued càdlàg functions with a bound on the sectional variation norm (van der Laan [2015]). As in van der Laan [2023], we denote this class as $D_M^{(0)}([0, 1]^d)$, where M is the bound on the sectional variation norm. The superscript (0) indicates zero-order, signifying that this class is derived from all linear approximations of zero-order splines. In contrast, higher-order spline HAL generalizes

to smoothness classes that are obtained as all linear combinations of higher-order splines, as precisely described by van der Laan [2023].

Assuming the true target function is an element of $D_M^{(0)}([0, 1]^d)$ is remarkably flexible, as this class of functions can capture a broad range of relationships, including non-linearities and even discontinuities. Nonetheless, one can restrict the function space by assuming an additive model, e.g. only including functions of one and two components. This corresponds to only using the basis functions for sets S of size 1 and 2 in the above representation of a càdlàg function. We denote this restricted class as $D_M^{(0)}(\mathcal{R}^0)$, referring to all linear combinations of zero-order splines identified by \mathcal{R}^0 , following the notation introduced by van der Laan [2023].

Let $L(Q)(O)$ be a loss function defining the functional parameter $Q(P) = \arg \min_{Q \in D_M^{(0)}([0, 1]^d)} PL(Q)$, where $Pf \equiv \int f(o)dP(o)$. The first step of the zero-order HAL is to define a rich set of zero-order spline basis functions, \mathcal{R}^0 , so that the linear span $D^{(0)}(\mathcal{R}^0) = \{\sum_{j \in \mathcal{R}} \beta(j)\phi_j : \beta\}$ provides a close enough approximation of $D^{(0)}([0, 1]^d)$.

In a typical zero-order HAL implementation, the observed data is converted into a large set of zero-order spline basis functions. The function Q , within $D_M^{(0)}([0, 1]^d)$ and adhering to the constraint $\|Q\|_v^* < M$, is represented as $Q(x) = Q(0) + \sum_{s \subset \{1, \dots, d\}} \int_{(0(s), x(x))} Q(du(s), 0(-s))$, leading to an approximation:

$$Q_\beta(x) = \beta_0 + \sum_{s_1 \subset \{1, 2, \dots, d\}} \sum_{j=1}^n \beta_{s_1, j} \phi_{u_{s_1, j}}(x) = \Phi^0(x)\beta \quad (3)$$

with $\|\beta\|_1 = |\beta_0| + \sum_{s_1 \subset \{1, 2, \dots, d\}} \sum_{j=1}^n |\beta_{s_1, j}| < M$.

This approximation is a linear combination of zero-order basis functions $x \rightarrow \phi_{u_{s_1, j}}(x) = I(x_{u_{s_1, j}} \leq x_s)$, defined by support points $x_{u_{s_1, j}}$ from the observations, along with their corresponding coefficient $\beta_{s_1, j}$.

2.2.2 Higher-Order Splines HAL

van der Laan [2023] has generalized the zero-order spline HAL-MLE to higher-order splines HAL-MLE. The first-order HAL-MLE assumes the true target function is an element of $D^{(1)}([0, 1]^d) \subset D^{(0)}([0, 1]^d)$, where the first-order smoothness class $D^{(1)}([0, 1]^d)$ consists of functions Q . Each section Q_S of these functions is absolutely continuous w.r.t. Lebesgue measure $dx(S)$, and this derivative $Q_S^{(1)} \equiv dQ_S/dx(S)$ is itself a càdlàg function of bounded sectional variation. This means its sections Q_{S, S_2} have bounded variation for all $S_2 \subset S$. The sum over S of all these sectional variation norms of Q_S is defined as the first-order sectional variation norm $\|Q\|_{v, 1}^*$.

van der Laan [2023] also provides a representation of $D^{(1)}([0, 1]^d)$ where each function is a linear combination of first-order splines, and the L_1 -norm of the corresponding coefficients equals the first-order sectional variation norm. First-order splines $\phi_u^1(x) = \prod_{j=1}^d \phi_{u_j}^1(x_j)$ are tensor products of univariate first-order splines $\phi_{u_j}^1(x_j) = I(x_j \geq u_j)(x_j - u_j)$ indexed by a knot-point u_j . For instance, $\phi_0^1(x_j) = x_j$ is a main term, and correspondingly $\phi_0^1(x) = \prod_{j=1}^d x_j$.

Specifically, it is shown that $Q \in D^{(1)}([0, 1]^d)$ can be represented as

$$Q(x) = \sum_{s_1 \subset \{1, \dots, d\}} \phi_0^1(x(s_1))Q_{s_1}^{(1)}(0(s_1)) + \sum_{s_1, s_2, s_1 \subset s_2} \phi_0^1(x(s_1/s_2)) \int \phi_{u(s_2)}(x(s_2))Q_{s_1, s_2}^{(1)}(du(s_2)).$$

The leading term is a linear combination of main terms x_j and their interactions $\prod_{j \in s_1} x_j$. The integral term is an infinite sum of tensor products over coordinates in S_2 of first-order splines, with a subset S_2/S_1 of them having zero knot-point.

The first-order smoothness HAL approximates any $Q \in D_M^{(1)}([0, 1]^d)$ with a linear model in first-order splines:

$$Q_\beta(x) = \Phi^1(x)\beta \quad \text{with} \quad \|\beta\|_1 < M,$$

with L_1 -norm of its coefficients bounded by M . The first-order spline function with a knot point $u \in [0, 1]^d$ is $\phi_u^1(x) = \int_{(u, x)} \phi_{u_1}^0(x)d\mu(u_1)$, so that it is obtained as a primitive of the zero-order splines. This key step uses the zero-order spline representation of Q , inputs the zero-order spline representation for its $dQ_S/dx(S)$, and rewrites the resulting expression using the fact that primitives of zero-order splines become first-order splines.

For example, if $d = 1$, $\phi_u^1(x) = (x - u)\mathbb{I}(x \geq u)$. If $d = 2$, $\phi_u^1(x) = (x_1 - u_1)(x_2 - u_2)\mathbb{I}(x_1 \geq u_1, x_2 \geq u_2)$. The parametric part for $d = 2$ includes all the first-order splines with knot points at zero which are x_1, x_2, x_1x_2 , and the linear combination includes $(x_1 - u_1)\mathbb{I}(x_1 \geq u_1)$, $(x_2 - u_2)\mathbb{I}(x_2 \geq u_2)$, and $(x_1 - u_1)(x_2 - u_2)\mathbb{I}(x_1 \geq u_1, x_2 \geq u_2)$. If $d = 3$, the parametric part includes $x_1, x_2, x_3, x_1x_2, x_1x_3, x_2x_3, x_1x_2x_3$; and the linear combination includes $(x_1 - u_1)\mathbb{I}(x_1 \geq u_1)$, $(x_2 - u_2)\mathbb{I}(x_2 \geq u_2)$, $(x_3 - u_3)\mathbb{I}(x_3 \geq u_3)$, their pairwise products, and the triple product. Similarly, for $d = 4, 5, \dots$, the parametric part and the linear combination can be constructed analogously by extending the dimensions and interactions.

Extending beyond the first order, HAL can be generalized to accommodate k -th order smoothness classes $D^{(k)}([0, 1]^d)$, where $k = 1, 2, \dots$. Functions in $D^{(k)}([0, 1]^d)$ can be approximated by a finite linear combination of k -th order splines. The L_1 -norm corresponds with the sum over all k -th order derivatives of its sectional variation norms, which is called the k -th order sectional variation norm. For comprehensive proofs and further specifics, we refer to the work by van der Laan [2023].

Minimizing loss

A crucial element of the 0- order HAL-MLE is to begin with a sufficiently rich finite set of zero-order spline basis functions. In the typical HAL implementation in the context of regression, where $Q(P) = E_P(Y | X)$, the initial set of basis functions is defined as $x(S) \rightarrow \phi_{X_i(S)}^0(x(S))$, for $i = 1, \dots, n$, and $S \subset \{1, \dots, d\}$. This initial set also provides the basis for generating the initial set of basis functions for the first-order HAL-MLE and higher order, with the inclusion of the zero-knot points as implied by the representation. van der Laan [2023] demonstrated that this finite-dimensional linear model provides an $O(n^{-1/2})$ supremum norm approximation for any function $Q \in D_M^{(0)}([0, 1]^d)$ for a given $M < \infty$, under a weak condition.

The HAL-MLE is defined as the minimizer of the empirical risk over the linear model under the constraint that the L_1 -norm is bounded by some M , which can then be selected with cross-validation. Not all subsets s need to be included, allowing the use of a subset of this maximally rich set of basis functions, corresponding to fitting a particular additive model. In addition, the set of knot-points for each section can be reduced, since n is often larger than needed.

For example, if our target function $Q(P) = \mathbb{E}_P(Y|X)$, a natural loss function is $L(Q)(O) = (Y - Q(X))^2$. Consequently, the zero-order HAL-MLE can be represented as $Q_n^{M_n} = \sum_{s,j} \beta_n(s,j) \phi_{s,j}^0$, where

$$\beta_n = \arg \min_{\beta, \|\beta\|_1 \leq M_n} L \left(\sum_{s,j \in \mathcal{J}_n(s)} \beta_n(s,j) \phi_{s,j}^0 \right).$$

Here, $\mathcal{J}_n(s)$ is the collection of support points of the s -specific section $Q_{n,s}$ of Q_n , and M_n the data-adaptively chosen bound for the sectional variation norm, determined through cross-validation (CV) by HAL. HAL effectively optimizes the trade-off between bias and variance concerning the conditional mean (prediction) model.

As proven in van der Laan [2017] and van der Laan [2023], the zero-order HAL achieves the rate of convergence $n^{-\frac{2}{3}} \log(n^d)$ and first-order HAL achieved $n^{-\frac{2}{5}}$ up till a power of $\log(n)$ factor. These rates of convergence are in loss-based dissimilarity, and for the k -th order HAL-MLEs with $k = 1, 2, \dots$, these rates hold for pointwise convergence to a normal limit distribution and in supremum norm.

Using data-adaptively transformed basis functions and selected M_n , this optimization is achieved through the existing GLMNET software (Friedman et al. [2021]). A rich set of HALs can be considered by exploring a variety of subsets of the full set of k -th order spline basis functions and by varying the degree k of the splines.

2.2.3 Undersmoothed HAL

The Highly Adaptive Lasso (HAL) method uses cross-validation (CV-HAL) to select the sectional variation norm bound, aiming to balance bias and variance for the true target function $Q(P_0)$. This method optimally trades off an average across all points of bias and variance, achieving an optimal rate of convergence with respect to loss-based dissimilarity $d_0(Q, Q_0) = P_0L(Q) - P_0L(Q_0)$, which generally corresponds with the square of an $L^2(P_X)$ -norm.

However, the cross-validated risk criterion for the cross-validation selector typically results in HAL-estimators that are overly biased for smooth features of the true curve. To address these issues, undersmoothed HAL was proposed by van der Laan et al. [2022].

Undersmoothing involves choosing an L_1 -norm bound M large enough to include 'sparse enough' basis functions in the model, akin to selecting a sufficiently small penalty, λ , in GLMNET. This enhances the model's ability to solve enough score equations, ensuring the linear span of these scores provides a good approximation of the efficient influence curve of the target parameter. If the target feature of interest is known, one could simply increase the L_1 -norm until

the efficient influence curve score equation is solved at the level $\sigma_n/(n^{1/2} \log n)$, where $\sigma_n/n^{1/2}$ is the standard error estimate based on the sample variance of the efficient influence curve.

For scenarios where the HAL is used for a variety of smooth features of the target function, a global undersmoothing criterion is preferred. This criterion selects an L_1 norm such that the standardized score equations $P_n \frac{d}{d\beta_n(s,j)} L(Q_n, \beta_n)$ of the working model $\{\sum_{(s,j), \beta_{n,cv}(s,j) \neq 0} \beta(s,j) \phi_{s,j}^0 : \beta\}$ selected by the cross-validated HAL remain at or below $\frac{1}{\log(n)}$. In practice, from a set of λ values smaller than the λ selected by cross-validation in the initial HAL fit, the largest λ meeting the global undersmoothing criteria is chosen. In the context of least squares regression, the criterion is defined as follows: Let \mathcal{S} denote the set of indices (s, j) , representing all basis functions identified during the initial HAL fit. For every (s, j) in \mathcal{S} , the primary goal is encapsulated mathematically by

$$|P_n(\phi_{s,j}(Y - \bar{Q}_{n,\lambda}))| \leq \frac{\hat{\sigma}_n(s,j)}{\sqrt{n} \log(n)} \quad (4)$$

where $\hat{\sigma}_n^2(s,j) = \text{Var}(\phi_{s,i}(Y - \bar{Q}_{n,\lambda_{cv}})) = \frac{1}{n} \sum_{k=1}^n [(y_k - \hat{y}_{\lambda_{cv}}) \phi_{s,i} - \frac{1}{n} \sum_{k=1}^n (y_k - \hat{y}_{\lambda_{cv}}) \phi_{s,i}]^2$.

2.2.4 Undersmoothed Smoothness-Adaptive HAL

In practical scenarios, the exact shape of the dose-response curve often remains unidentified, posing challenges in determining the optimal level of smoothness and other crucial hyperparameters for the Highly Adaptive Lasso (HAL) fit, which are influenced by the curve's characteristics. To address these challenges, the Smoothness-Adaptive HAL, introduced by Van der Laan (2023), leverages the discrete Super Learner to select the smoothness order adaptively.

The Smoothness-Adaptive HAL utilizes the discrete Super Learner to identify the appropriate smoothness order and other relevant hyperparameters, such as the number of knots, within a cross-validation framework. This approach offers a sophisticated and data-driven method for hyperparameter selection in the context of dose-response curve modeling.

Once the optimal HAL configuration is determined, the method employs an undersmoothing strategy to further refine the HAL fit. This deliberate undersmoothing step is designed to enhance the performance and accuracy of the final model, providing a robust fit that accommodates the nuances of the dose-response relationship.

2.3 Pointwise Asymptotic Normality

In van der Laan [2023], it is shown that the HAL-MLE Q_n or its relax version is asymptotically normally distributed, allowing for the construction of confidence intervals for $Q_0(x)$ for a given x .

To understand this result, we note that HAL selects a working model $D^{(k)}(\mathcal{R}_n) = \{\sum_{j \in \mathcal{R}_n} \beta(j) \phi_j : \beta\}$, where \mathcal{R}_n is the set of basis functions with non-zero coefficients the HAL fit. We define Q_{0,\mathcal{R}_n} as the projection of Q_0 onto this working model, defined by $Q_{0,\mathcal{R}_n} = \arg \min_{Q \in D^{(k)}(\mathcal{R}_n)} P_0 L(Q)$.

Suppose we consider the relax HAL, knowing that $Q_n \in D^{(k)}(\mathcal{R}_n)$ is an actual MLE over $D^{(k)}(\mathcal{R}_n)$. We can then analyze $Q_n - Q_{0,\mathcal{R}_n}$ as we would analyze an MLE for a parametric working model. In the proof, van der Laan uses an orthonormal basis of $\{\phi_j : j \in \mathcal{R}_n\}$, orthonormalized so that the information matrix under P_0 is diagonal. For log-likelihood behaving loss functions, this corresponds with choosing the basis so that the scores of $\beta(j)$, $j \in \mathcal{R}_n$, are orthogonal in $L^2(P_0)$. Due to the information matrix being diagonal, it follows that $\sum_{j \in \mathcal{R}_n} (\beta_n - \beta_{0,\mathcal{R}_n})(j) \phi_j$ is, in first-order, an empirical mean of an influence curve, which is a linear combination of the scores of $\beta(j)$, $j \in \mathcal{R}_n$. The variance of this influence curve increases with J_n , where J_n is the size of \mathcal{R}_n . Consequently, $(n/J_n)^{1/2}(Q_n - Q_{0,\mathcal{R}_n})(x)$ converges to a normal distribution. Moreover, the linear approximation allows for empirical process to show supremum norm convergence of $Q_n - Q_{0,\mathcal{R}_n}$ at this rate $(J_n/n)^{1/2}$ up till a log n -factor.

In a separate proof, van der Laan [2023] establishes a uniform approximation error of a finite dimensional J_n -dimensional working model $D^{(k)}(\mathcal{R}(J_n))$ with respect to $D^{(k)}([0, 1]^d)$, behaving as $O(1/J_n^{k+1})$ up till log J -factors, for $k = 1, 2, \dots$. This means that one can select $O(J)$ k -th order spline basis functions to uniformly approximate any $Q \in D_M^{(k)}([0, 1]^d)$ with an error of $O(1/J^{k+1})$ up till log J -factors. HAL can select such a working model from a rich initial model, explaining its convergence at the optimal rate $n^{-k^*/(2k^*=1)}$, up till log n -factors, with $k^* = k + 1$, $k = 0, 1, 2$. Moreover, cross-validation selects the right size J_n to achieve the optimal trade-off between standard error $(J/n)^{1/2}$ and bias $\sim 1/J^{k+1}$, resulting in a working model of size $J_n \sim n^{1/(k^*+1)}$ up till log n -factors.

For a full technical proof of these results, we refer to van der Laan [2023]. One technical component is that the above sketched proof works when \mathcal{R}_n is externally selected, but the data dependence of \mathcal{R}_n causes problems for the CLT

argument. To address this, van der Laan [2023] works with an independent working model $D^{(k)}(\mathcal{R}_{n,0})$, where $\mathcal{R}_{n,0}$ is the selected working model when HAL is applied to an independent sample from P_0 (independent from the actual sample). It is shown that the actual HAL-MLE still solves the score equations of this independent working model with sufficient precision so that the MLE proof above can be carried out.

In conclusion, HAL, relaxed HAL, and user-supplied sieve MLEs yield pointwise asymptotically normally distributed estimators at dimension-free rates of convergence, ignoring $\log n$ -factors. One can also construct simultaneous confidence bands at the same rate. The key factors enabling these results are the remarkable dimension-free uniform approximation errors of linear combinations of k -th order splines; the fact that HAL is an MLE for the data adaptively selected working model; and that HAL's ability to select a sparse set of basis functions that yields this uniform approximation error, unlike a sieve MLE which cannot adapt the choice to the true target function.

2.4 Define Target Parameter

Consider an observational research or an experiment, where we observe a continuous exposure or treatment variable A , either a continuous or binary outcome Y , and a set of covariates W for n randomly sampled subjects. Let $O = (W, A, Y)$, which is a Euclidean random variable with dimension d , following the true data generating distribution (DGD) $P_0 \in \mathcal{M}^{NP}$, where \mathcal{M}^{NP} is a realistic nonparametric model. Suppose we have n copies of i.i.d. observations of O , denoted as O_1, \dots, O_n .

To investigate the causal impact of a treatment variable A on an outcome Y , we focus on estimating the marginal causal dose-response curve. This requires defining a statistical target parameter that captures the causal relationship. Specifically, we introduce the target parameter

$$\Psi_P(a) = \mathbb{E}_P Y(a) = \mathbb{E}_P \mathbb{E}_P[Y|W, A = a],$$

which maps the data generating distribution (DGD) to the real line. This parameter represents the expected outcome of Y when the treatment A is set to a specific value a , across a continuum of treatment levels within its possible range. It can be interpreted as the expected outcome when everyone in the target population has the treatment level a over a set of selected points on the curve, under the randomization assumption and the positivity assumption. We use $\Psi_0 = \Psi(P_0)$ to denote the estimand, which is the underlying ground truth.

If Y is continuous, we define $Q_P(W, A) := \mathbb{E}[Y|W, A]$ as the conditional mean of Y given baseline covariates W and treatment A . Thus, $\Psi_P(a) = \mathbb{E}Q(W, A = a) = \int_w Q(w, a)dP(w)$. Here, Q is a functional parameter of the data distribution as $Q : \mathcal{M} \rightarrow Q(\mathcal{M}) = \{Q(P) : P \in \mathcal{M}\}$. Our plug-in estimator is of the form $\hat{\Psi}(a) = \frac{1}{n} \sum_{l=1}^n \hat{Q}(W_l, a)$, where \hat{Q} is a HAL-MLE represented as a linear combination of basis functions according to the working model selected by HAL. When Y is binary, we first parametrize $E_P(Y | W, A) = 1/(1 + \exp(-Q_P(W, A)))$ so that Q_P now plays the role of $\text{Logit}E_P(Y | A, W)$. This allows Q_P to be modeled as a linear combination of basis functions, while still respecting the probability constraint.

2.5 HAL-based Plugin Estimator and Delta-based Confidence Intervals:

Using HAL to estimate the functional parameter Q , we subsequently employ the learned working model $D^{(k)}(\mathcal{R}_n)$ to obtain inference as if this working model was a priori specified. Our HAL-MLE is an MLE of this working model, which holds exactly for relax-HAL and holds up to negligible regularization bias for HAL. We estimate the variance of $Q_{\beta_n}(x) = \sum_{j \in \mathcal{R}_n} \beta_n(j) \phi_j(x)$ by applying the delta method, in line with the formal asymptotic normality results discussed in van der Laan [2023].

For continuous outcomes (Y), HAL solves the score equation $P_n \frac{d}{d\beta} L(Q_\beta) = 0$ such that $\beta_n = \arg \min_{\beta} P_n L(Q_\beta) = \arg \min_{\beta} \mathbb{E}_{P_n} [(Y - \Phi^T(A, W)\beta)^2]$. Here, $\Phi_i = \Phi(A_i, W_i)$ is the basis vector transformed from treatment A and baseline covariates W for observation i . For a fixed working model, the coefficient vector β_n is asymptotically linear with influence curve $IC_{\beta, P}(O_i) = \mathbb{E}_P[\Phi_i^T \Phi_i]^{-1} \Phi_i^T (Y_i - \Phi_i^T \beta)$. Using the delta method, our plug-in estimator $1/n \sum_i \beta_n^T \Phi(a, W_i)$ is asymptotically linear with its influence curve, which is an inner product of its gradient with respect to the coefficients and the influence curve of the coefficients:

$$IC_{\psi_{a, P}}(O_i) = \frac{1}{n} \sum_{l=1}^n \Phi(a, W_l)^T IC_{\beta, P}(O_i). \quad (5)$$

This influence curve represents the contribution from the estimator Q_n of Q_{0, \mathcal{R}_n} . The other component of the influence curve is given by $\beta^\top \Phi(a, W) - E_W \beta^\top \Phi(a, W)$.

Likewise, for binary outcomes (Y), HAL solves the score equation $P_n \frac{d}{d\beta} L(Q_\beta) = 0$ such that $\beta_n = \arg \min_{\beta} - \mathbb{E}_{P_n} [Y \log(\psi_\beta + (1 - Y) \log(1 - \psi_\beta))]$, where $\psi_\beta = \frac{1}{1 + e^{\Phi^T \beta}}$ is the predicted probability of $Y = 1$. The coefficients β_n is asymptotically linear with influence curve $IC_{\beta, P}(O_i) = \mathbb{E}_P [\Phi_i^T \frac{\Phi_i e^{-\Phi_i^T \beta}}{(1 + e^{\Phi_i^T \beta})^2}]^{-1} \Phi^T (Y_i - \psi_{\beta, i})$. By delta method, $\psi_n(a)$ is asymptotically linear with influence curve

$$IC_{\psi(a), P}(O_i) = \frac{1}{n} \sum_{l=1}^n \frac{\Phi(a, W_l) e^{-\Phi(a, W_l)^T \beta(P)}}{(1 + e^{\Phi(a, W_l)^T \beta(P)})^2} IC_{\beta, P}(O_i). \tag{6}$$

The full influence curve also has a contribution from the empirical mean over W given by $\psi_\beta(a, W) - E_P \psi_\beta(a, W)$.

With the influence curve of our HAL-based plugin estimator at each treatment point a , we estimate the variance as $\hat{\sigma}_n^2(a) = \frac{1}{n} \text{Var}(IC_{\psi(a), P}(O_i))$. The corresponding 95% confidence interval is given by $\psi_n(a) \pm 1.96 \hat{\sigma}_n(a)$.

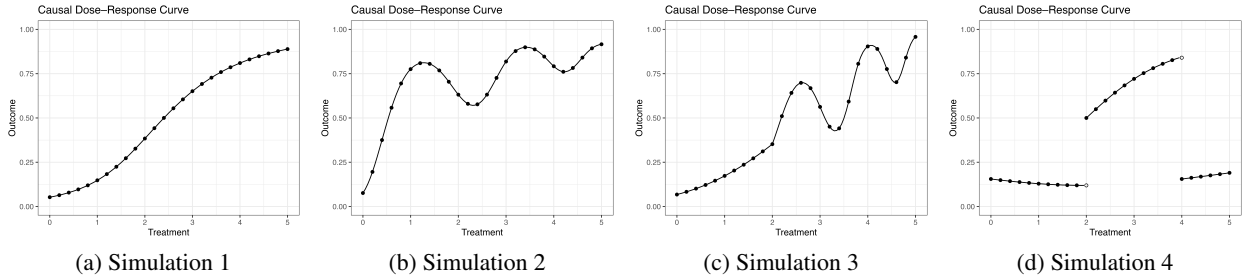
These parametric working model-based confidence intervals are asymptotically valid according to the theoretical results in van der Laan (2023). They ignore the bias $Q_{P, \mathcal{R}_n} - Q_P$ and primarily provide inference for the projection Q_{P, \mathcal{R}_n} . However, with appropriate undersmoothing, this bias becomes asymptotically negligible relative to the standard error.

2.6 Simulation settings

To assess the effectiveness of undersmoothed HAL-based estimations in determining the marginal dose-response curve $\mathbb{E} Y(a)$, Monte Carlo simulations were conducted on four unique curves. These curves varied in complexity, continuity, and discontinuity.

Figure 1 illustrates the true marginal dose-response curve $\mathbb{E} Y(a)$ for each of these simulations. In Simulation 1, the curve is smooth and monotonically increasing, albeit non-linear. For Simulation 2, the curve exhibits several oscillations. Simulation 3 is a composite of the characteristics found in both simulations 1 and 2: the initial half of the curve is smooth, akin to simulation 1, whereas the segment where a lies between 2 and 5 demonstrates oscillations. In simulation 4, the curve is characterized by two discontinuities at $a = 2$ and $a = 4$, with non-zero values exclusively within this interval.

Figure 1: True causal dose-response curves



These four simulations were executed under a consistent setting. For each simulation, n independent and identically distributed (i.i.d.) copies of the data $O = (W, A, Y)$ were simulated. Here, W represents a baseline covariate, A signifies the treatment level dependent on W and varies continuously between 0 and 5, and Y indicates the outcome of interest, denoting the occurrence of an event.

In each simulation, we generated 500 datasets of sizes 200, 500, 1000, and 5000, following the data generating processes detailed in Table 3 in Appendix A. These datasets were fitted by six variations of Highly Adaptive Lasso (HAL), distinguishing each model by its approach to smoothness and method of regularization. These included: (1) zero-order smoothness with cross-validation (CV), (2) zero-order smoothness with undersmoothing, (3) first-order smoothness with CV, (4) first-order smoothness with undersmoothing, (5) adaptive smoothness with CV, and (6) adaptive smoothness with undersmoothing. The zero-order models were configured using the default number of knots from the `hal9001` R package, catering to scenarios with indeterminate smoothness orders and knot configurations. In contrast, the first-order models were trained with a smaller number of knots, which is more appropriate for our simulated scenarios with fewer dimensions and less complexity, while the adaptive models were designed to dynamically adjust to data complexity, enhancing flexibility in the fitting process. For each simulation setting, oracle standard deviations were calculated across the 500 repetitions, with corresponding confidence intervals derived, to evaluate the estimators' asymptotic behaviors.

These variants are evaluated based on five metrics from both perspectives of delta-method based inferences and Monte Carlo oracle performances: coverage rates of 95% confidence intervals, bias, SE, bias/SE ratio, and mean squared error (MSE). QQ-plots were generated to inspect the sampling distribution’s normality. To evaluate the selected penalties’ by CV and global undersmoothing criteria, comparisons were made against a grid of penalties. Ultimately, the study juxtaposed the performance of Globally Undersmoothed Smoothness-Adaptive HAL against established models such as the general adaptive model (GAM), polynomial regression model, and the npcausal by Kennedy et al. [2017].

3 Results

In this section, we present our key findings, structured around four pivotal themes: (1) Cross-Validation (CV) and the implications of Undersmoothing, (2) the Evaluation of Undersmoothing Criteria, (3) an Analysis of the Smoothness-Order Adaptive HAL, and (4) a Comparative Assessment with Other Methods. To substantiate our findings, we will reference one or two simulations as illustrative examples. Detailed results, accompanied by comprehensive plots for all simulations and sample sizes, are provided in the Appendix.

3.1 CV and Undersmoothing

Table 1 presents the average point-wise performance of estimators at two points on the curve in simulations, using the first order Highly Adaptive Lasso (HAL) with lambda determined by both Cross-Validation (CV) and Undersmoothing criteria for a sample size of 1000. Figures 2 and 3 illustrate the performance curves for simulations 1 and 3, respectively. Across all simulations, the Undersmoothing criteria consistently selected a greater number of bases than the CV selectors. In scenarios where the true dose-response curve is straightforward, as in simulation 1, negligible differences between the two criteria were observed. The delta-method based confidence intervals’ average coverage rate across treatment points on the curve, over 500 Monte Carlo repetitions, achieved 94.2% and 95.7% for CV and Undersmoothing selectors, respectively, with both methods yielding an average bias of approximately 0.02. Despite Figure 2 indicating a slight superiority of CV over the Undersmoothing selector, this advantage is minimal.

On the contrary, in simulation 3, characterized by a more complex dose-response curve, the Undersmoothing approach significantly outperformed the CV method, especially at curve points that enhance complexity. Here, the CV method reached an oracle coverage rate of 83.1% with an average bias of 0.048, while the Undersmoothing method achieved a 90.4% oracle coverage rate with a lower average bias of 0.044. As illustrated in Figure 3, estimators using the undersmoothed HAL approach exhibited reduced bias and improved confidence interval coverage at points of increased curve complexity.

Furthermore, the delta-method based variance estimates were found to closely approximate the oracle variance across all simulations, as evidenced in Figures 2 and 3, with the performances derived from delta-method based inference represented by dashed lines and oracle performances by solid lines.

Table 1: Average pointwise performances of HAL-based plugin estimator at A = 2 and 4 on dose-response curves n = 1000

Simu	A	Selector	Bias	MSE	Oracle			Delta-method		
					CI Coverage	Bias/SE	SE	CI Coverage	Bias/SE	SE
1	2	CV	0.021	0.001	0.968	0.759	0.028	0.954	0.787	0.026
		U	0.026	0.001	0.976	0.725	0.036	0.946	0.787	0.033
	4	CV	0.019	0.001	0.934	0.820	0.024	0.952	0.790	0.024
		U	0.023	0.001	0.952	0.795	0.030	0.958	0.791	0.029
2	2	CV	0.017	0.000	0.838	1.044	0.017	0.950	0.790	0.022
		U	0.020	0.001	0.904	0.901	0.024	0.959	0.765	0.026
	4	CV	0.016	0.000	0.830	1.191	0.015	0.940	0.815	0.020
		U	0.017	0.000	0.796	1.323	0.015	0.943	0.829	0.021
3	2	CV	0.058	0.004	0.576	1.856	0.033	0.662	1.682	0.034
		U	0.050	0.004	0.768	1.354	0.041	0.834	1.180	0.043
	4	CV	0.098	0.012	0.346	2.910	0.035	0.564	1.807	0.054
		U	0.072	0.008	0.562	2.046	0.036	0.832	1.138	0.063
4	2	CV	0.183	0.035	0.024	4.685	0.042	0.008	4.580	0.040
		U	0.196	0.041	0.108	3.519	0.059	0.028	3.982	0.049
	4	CV	0.334	0.115	0.000	6.020	0.057	0.000	5.388	0.062
		U	0.315	0.105	0.004	5.087	0.064	0.004	4.408	0.072

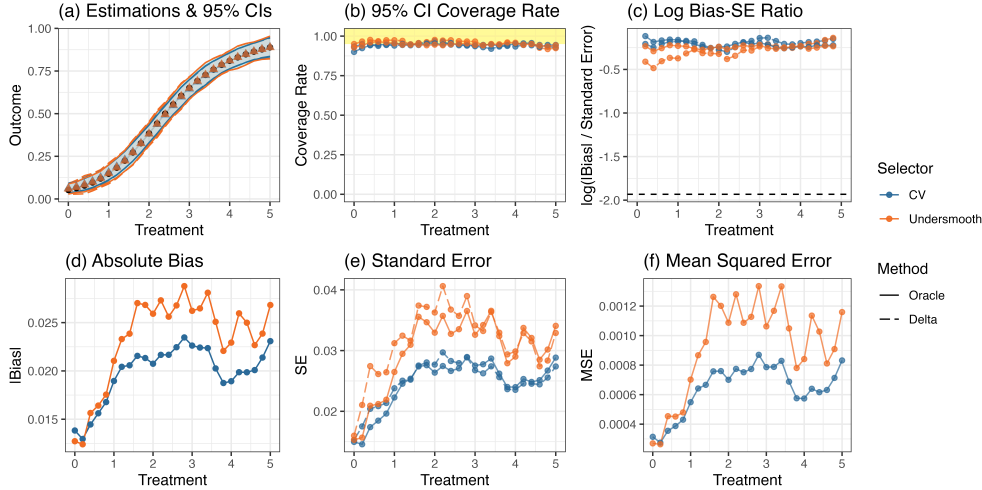


Figure 2: Performances in Simulation 1, $n = 1000$

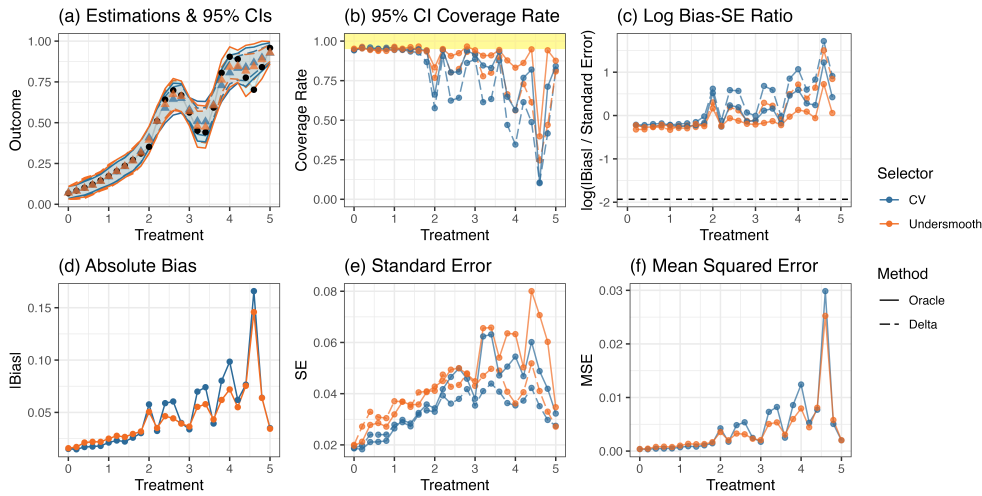


Figure 3: Performances in Simulation 3, $n = 1000$

3.2 Evaluation of Undersmoothing Criteria

Figure 4 plots the detailed estimator performances across a spectrum of penalty candidates, delineated at five points along the dose-response curve in simulation 3, with a sample size of 1000. Each subplot illustrates a different performance metric and a corresponding treatment value a as we adjust the penalty values; the selected penalties by the undersmoothing criteria are shown as orange dashed lines, while the CV selected penalties are depicted as blue dashed lines.

Moving along the penalty spectrum, we observe an increase in standard errors (SE) and coverage rates of 95% CIs with decreasing penalty values. Notably, at certain curve points, such as $a = 0.4$ and $a = 1.4$, there is a monotonic increase in both bias and MSE as penalties increase past the CV selected value. In contrast, at other points, bias and MSE initially decrease to reach a minimum before increasing again.

Across the different scenarios represented by varying a values, the undersmoothing criteria manage to maintain a balanced performance, neither excessively penalizing nor underfitting, as evidenced by the convergence of trends in bias, standard error, and MSE towards optimal values at the selected penalty.

HAL-based plug-in estimator performances

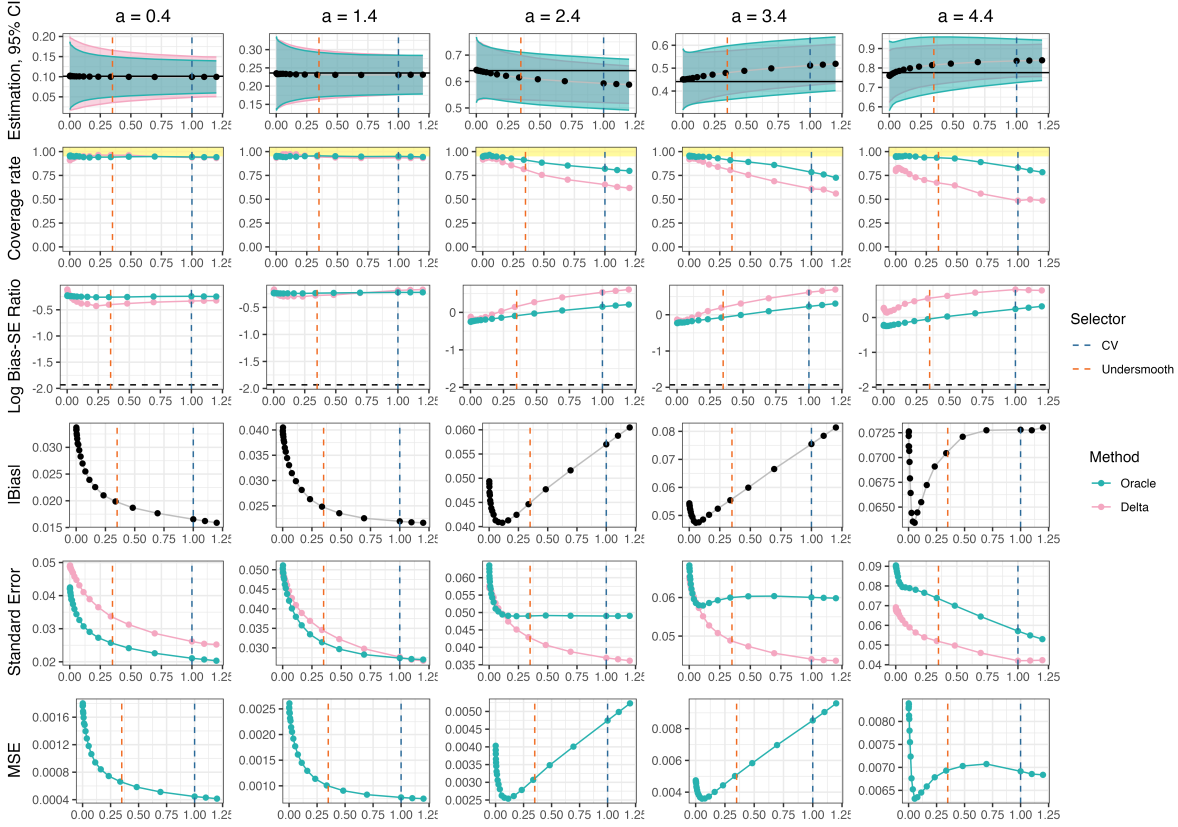


Figure 4: Pointwise Performances on 5 example points of a grid of penalties in Simulation 3, $n = 1000$

3.3 Analysis of the Smoothness-Order Adaptive HAL

Figures 5 and 6 provide a comprehensive evaluation. Figure 5 elucidates the oracle performance of the HAL-based plugin estimator for simulations 1 and 3, across varying smoothness orders (0 to 4) and contrasts the outcomes for smaller ($n=200$) and larger ($n=5000$) sample sizes. Figure 6 offers insights into the mean cross-validation (CV) risks across testing sets within four simulation settings, encompassing a spectrum of sample sizes.

In simulation 1, regardless of the sample size, the first-order smoothness estimators consistently exhibit superior performance compared to other smoothness orders. This is evident from the plots in both Figures 5 and 6. The adaptability of the method is highlighted by the fact that the Smoothness-Order Adaptive HAL predominantly favored the first-order smoothness, selecting it in 70.6% of the 500 Monte Carlo iterations with a sample size of 200 and in 98.4% of the iterations with a sample size of 5000.

For simulation 3, intriguing dynamics emerge. With smaller sample sizes (200, 500, and 1000), zero-order smoothness estimators showed slightly superior performance on the dose-response curve relative to first-order smoothness. However, the average CV risks were either marginally higher or similar to those of the first-order. Conversely, with a larger sample size, the first-order smoothness becomes increasingly effective, outperforming other orders across all evaluation metrics. The decision-making capacity of the Smoothness-Order Adaptive HAL is in harmony with these observations. For smaller sample sizes of 200, 500, and 1000, the HAL chose first-order smoothness 67.4%, 62.1%, and 56% of the time, respectively. Notably, for the largest sample size of 5000, the HAL demonstrated a definitive preference, selecting the first-order smoothness in every iterations (100%).

3.4 Comparative Assessment with Other Methods

Figure 7 displays the oracle pointwise performances of four estimators in estimating the dose-response curve across four different simulations with a sample size of 5000. The estimators are the undersmoothed Highly Adaptive Lasso-based

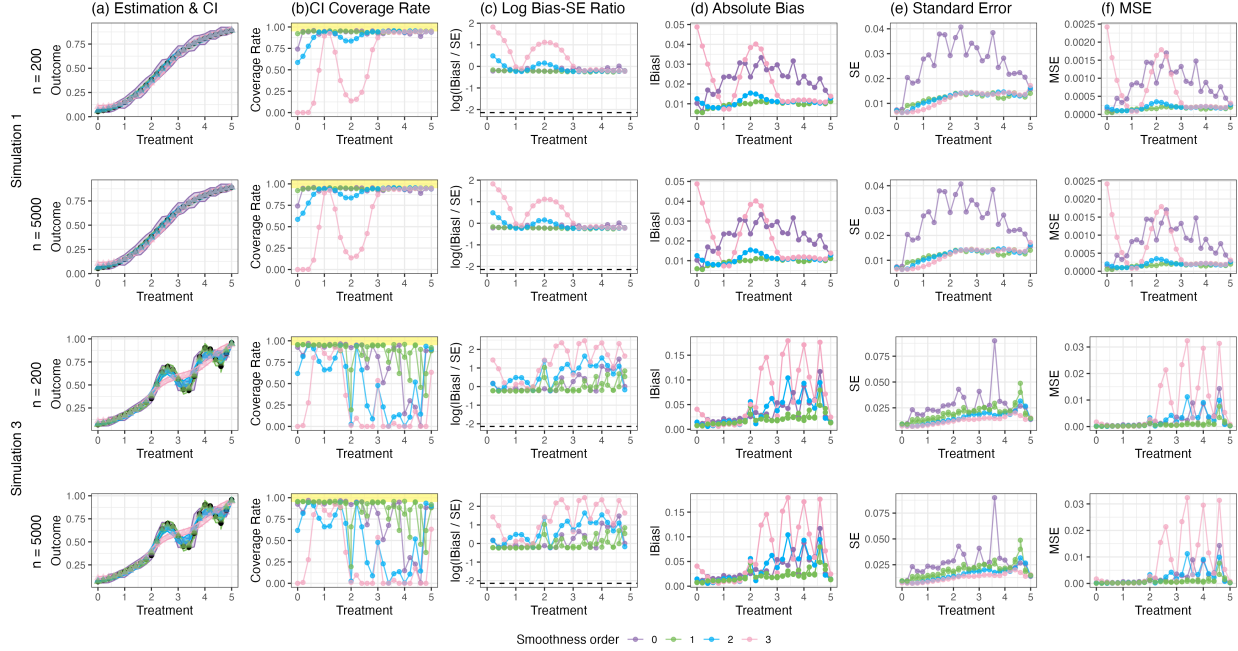


Figure 5: Oracle Performance of Estimators Across Simulations 1 and 3 with Sample Sizes of 200 and 5,000

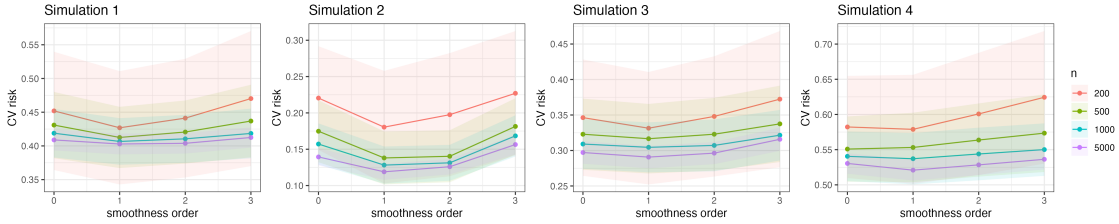


Figure 6: CV risks in 4 simulations

plug-in estimator (HAL) in green, Generalized Additive Model-based plug-in estimator (GAM) in orange, polynomial model-based estimator (Poly) in pink, and the nonparametric causal inference estimator (npcausal) in purple. In addition, Table 2 lists the average pointwise oracle and delta-method-based performances of the four estimators. It provides a quantitative assessment of the absolute bias, MSE, CI coverage, bias/SE, and SE across each simulation.

In Figure 7(a), the estimations and oracle confidence intervals (CI) are shown. The HAL, GAM, and npcausal estimators appear to closely follow the trend of the simulated outcomes, whereas the polynomial model does not align as consistently with the simulated outcomes. The CI coverage rate in Figure 7(b) indicates that, for Simulation 1, the HAL estimator achieved an average oracle CI coverage rate of 94.6% and a delta-method based CI coverage rate of 96.9%. The other methods did not reach the 95

The performance of the estimators varied across the simulations. In the more complex Simulation 3, the HAL estimator’s average oracle and delta-method CI coverage rates were 90.9% and 90.3%, respectively, with the other estimators not achieving an average CI coverage above 80%.

The absolute bias shown in Figure 7(d) demonstrates that the HAL estimator had lower average absolute bias across all simulations, with values of 0.012, 0.01, 0.019, and 0.042 for Simulations 1 to 4, respectively. The npcausal estimator followed, with slightly higher absolute bias values in each respective simulation.

In terms of the mean squared error (MSE) and log bias-standard error (SE) ratio, depicted in Figures 7(e) and 7(f), the HAL estimator presented the smallest values in all simulations, indicating a lower variance and bias ratio than the other estimators.

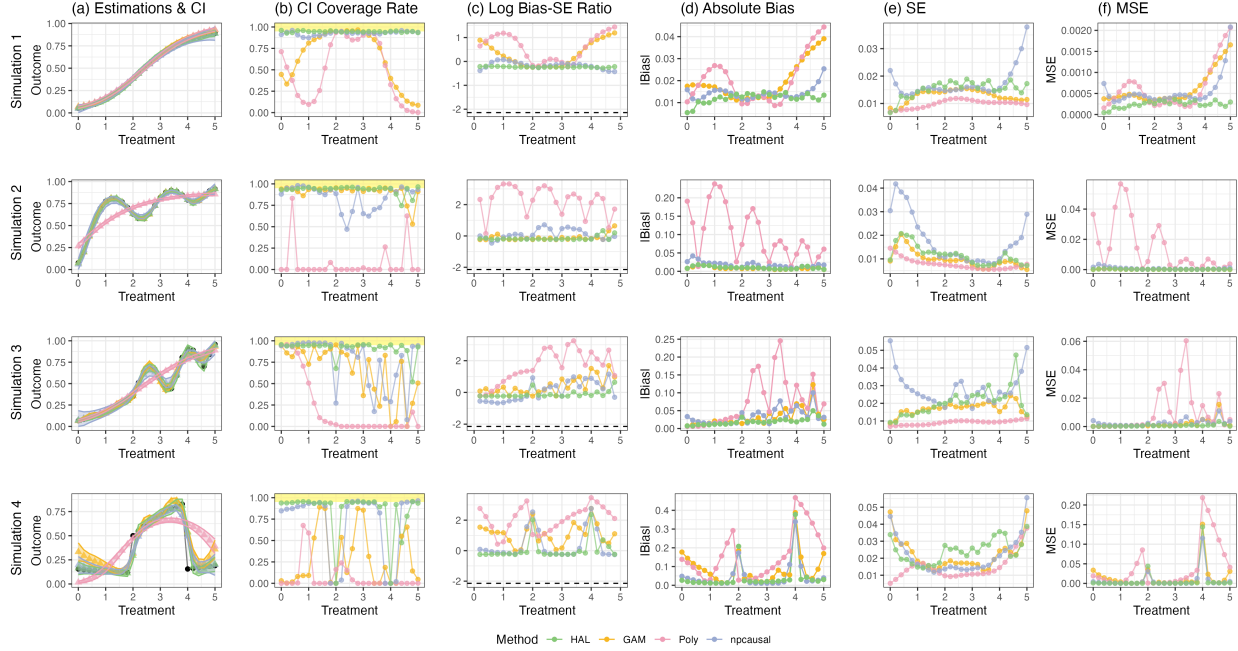


Figure 7: Oracle Performances of 4 estimators in 4 simulations, $n = 5000$

Simu	Method	Oracle				Delta-method			
		Bias	MSE	CI Coverage	Bias/SE	SE	CI Coverage	Bias/SE	SE
1	HAL	0.012	0.000	0.946	0.792	0.015	0.969	0.710	0.017
	npcausal	0.014	0.001	0.927	0.841	0.017	0.868	1.065	0.014
	GAM	0.019	0.001	0.653	1.621	0.013	0.704	1.524	0.015
	Poly	0.021	0.001	0.498	2.153	0.010	0.593	1.848	0.012
2	HAL	0.010	0.000	0.930	0.860	0.012	0.889	0.958	0.012
	npcausal	0.018	0.001	0.850	1.112	0.018	0.706	1.499	0.013
	GAM	0.009	0.000	0.907	0.919	0.010	0.876	0.998	0.009
	Poly	0.100	0.015	0.070	12.769	0.008	0.065	14.020	0.007
3	HAL	0.019	0.001	0.909	0.916	0.020	0.903	0.898	0.022
	npcausal	0.034	0.003	0.764	1.260	0.028	0.614	1.900	0.020
	GAM	0.031	0.002	0.658	1.745	0.017	0.672	1.712	0.017
	Poly	0.073	0.010	0.214	7.528	0.009	0.253	6.068	0.011
4	HAL	0.042	0.008	0.843	1.522	0.024	0.840	1.483	0.027
	npcausal	0.048	0.008	0.708	2.490	0.021	0.662	2.923	0.017
	GAM	0.087	0.014	0.281	3.807	0.022	0.338	3.243	0.025
	Poly	0.158	0.042	0.072	11.135	0.015	0.096	11.458	0.015

Table 2: Average Performances of 4 estimators in 4 simulations, $n = 5000$

4 Discussions

In our series of simulations and the application of various estimation criteria, we observed the insightful performances of different methods in dose-response estimation.

The choice between Cross-Validation (CV) and Undersmoothing criteria in selecting the penalty for the Highly Adaptive Lasso (HAL) is shown to have non-trivial implications on the estimation outcomes. The CV and Undersmoothing approaches exhibit comparable performances in simple scenarios, as observed in simulation 1, where the complexity of the dose-response curve is minimal. However, the distinction becomes pronounced in the presence of a more intricate curve structure, such as in simulation 3, where the Undersmoothing approach demonstrates its efficacy by achieving higher oracle coverage rates and lower average biases. This suggests that the Undersmoothing criteria might be preferable in cases where capturing complex curve features is critical. In addition, in exploring the impact of the

penalty spectrum on estimator performance, it's apparent that the undersmoothing criteria adeptly navigates the trade-off between bias and variance, achieving a balance which suggests an optimal fit across various points on the curve, which is crucial when dealing with diverse curve complexities. Moreover, the adaptability of the Smoothness-Order Adaptive HAL to different sample sizes and curve complexities also merits discussion. The first-order smoothness estimators' consistently superior performance, particularly for larger sample sizes, underscores the method's responsiveness to sample size and underlying curve smoothness.

The comparative assessment of the four estimators—HAL, GAM, Polynomial model (Poly), and nonparametric causal (npcausal) provided the evidence that the HAL-based plug-in estimator consistently outperforms the other methods across the simulations. With the highest CI coverage rates, lowest absolute biases, and smallest MSE values, the HAL-based plugin estimator demonstrates robustness, especially in the face of complex simulation scenarios. The other estimators, particularly the polynomial model, show considerable variability and do not maintain the same level of performance. Consequently, for the task of estimating dose-response curves, the HAL-based plug-in estimator emerges as a preferable choice due to its accuracy and reliability in capturing the true underlying patterns within the data.

5 Conclusions

In this study, we evaluated the robust performance of the Highly Adaptive Lasso (HAL)-based plugin estimator for estimating causal dose-response curves across multiple simulation scenarios. Our findings indicate that the HAL-based estimator outperforms traditional methods such as Generalized Additive Models (GAM) and polynomial modeling, as well as the more nuanced nonparametric causal inference method (npcausal) proposed by Kennedy et al. [2017]. The estimator's resilience to increasing complexity and adaptability to variations in sample size highlight its potential for broad application.

There are other estimation problems of interest, such as the inclusion of intermediate variables or multiple treatments. Although we did not include them in our simulations, we anticipate that the HAL-based plugin estimator can be extended to scenarios involving such mediators. Further research is needed to empirically validate this applicability. Additionally, our approach shows promise for expansion to other types of parameters, including non-pathwise differentiable ones like Conditional Average Treatment Effect (CATE), which could broaden its utility in causal inference research.

However, there are limitations to consider. The computational time for fitting a HAL, especially the smoothness-adaptive HAL, is relatively long. Moreover, 1.4% of simulations encountered invertibility problems when computing the estimated variance under the undersmoothing criteria due to highly correlated basis functions. Researchers in the Center for Targeted Machine Learning and Causal Inference are actively addressing these issues.

Our investigation demonstrated that employing the HAL-based plugin estimator with undersmoothing criteria effectively delineates complex dose-response relationships with valid inferences. The smoothness-order adaptive HAL, with its flexible nature, adeptly adjusts to diverse sample sizes and the intricacies inherent in dose-response curves, enhancing its utility in various practical contexts.

To facilitate the adoption of our methodology, we are developing a comprehensive R software package that will enable practitioners to harness the full capabilities of the HAL-based estimators. The source code for this package is available at <https://github.com/SeraphinaShi/HAL-DoseResponseCurve>, allowing researchers and analysts direct access to implement our estimator. The impending release of this fully developed package will empower researchers and analysts to leverage our findings and methodologies, potentially transforming practices in dose-response analysis and other applications requiring nuanced estimation methods.

References

- Mark J van der Laan. A generally efficient targeted minimum loss based estimator. 2015.
- Mark van der Laan. A generally efficient targeted minimum loss based estimator based on the highly adaptive lasso. *The international journal of biostatistics*, 13(2), 2017.
- Mark van der Laan. Higher order spline highly adaptive lasso estimators of functional parameters: Pointwise asymptotic normality and uniform convergence rates. *arXiv preprint arXiv:2301.13354*, 2023.
- Mark J van der Laan and Maya L Petersen. Direct effect models. *The international journal of biostatistics*, 4(1), 2008.
- Maya L Petersen, Sandra E Sinisi, and Mark J van der Laan. Estimation of direct causal effects. *Epidemiology*, pages 276–284, 2006.
- Donald B Rubin. Direct and indirect causal effects via potential outcomes. *Scandinavian Journal of Statistics*, 31(2): 161–170, 2004.

- Mark J Van der Laan, Sherri Rose, et al. *Targeted learning: causal inference for observational and experimental data*, volume 4. Springer, 2011.
- Donald B Rubin. *Matched sampling for causal effects*. Cambridge University Press, 2006.
- Mark J Laan and James M Robins. *Unified methods for censored longitudinal data and causality*. Springer, 2003.
- Alberto Abadie and Guido W Imbens. Large sample properties of matching estimators for average treatment effects. *econometrica*, 74(1):235–267, 2006.
- Joshua Angrist and Guido Imbens. Identification and estimation of local average treatment effects, 1995.
- James Robins. A new approach to causal inference in mortality studies with a sustained exposure period—application to control of the healthy worker survivor effect. *Mathematical modelling*, 7(9-12):1393–1512, 1986.
- Donald B Rubin. Bayesian inference for causal effects: The role of randomization. *The Annals of statistics*, pages 34–58, 1978.
- Peter C Austin and Elizabeth A Stuart. Moving towards best practice when using inverse probability of treatment weighting (iptw) using the propensity score to estimate causal treatment effects in observational studies. *Statistics in medicine*, 34(28):3661–3679, 2015.
- Miguel Angel Luque-Fernandez, Michael Schomaker, Bernard Rachet, and Mireille E Schnitzer. Targeted maximum likelihood estimation for a binary treatment: A tutorial. *Statistics in medicine*, 37(16):2530–2546, 2018.
- Mark J van der Laan, David Benkeser, and Weixin Cai. Efficient estimation of pathwise differentiable target parameters with the undersmoothed highly adaptive lasso. *The International Journal of Biostatistics*, (0), 2022.
- Peter J Bickel, Chris AJ Klaassen, Peter J Bickel, Ya’acov Ritov, J Klaassen, Jon A Wellner, and YA’Acov Ritov. *Efficient and adaptive estimation for semiparametric models*, volume 4. Springer, 1993.
- James M Robins, Miguel Angel Hernan, and Babette Brumback. Marginal structural models and causal inference in epidemiology. *Epidemiology*, pages 550–560, 2000.
- Romain Neugebauer and Mark van der Laan. Nonparametric causal effects based on marginal structural models. *Journal of Statistical Planning and Inference*, 137(2):419–434, 2007.
- Keisuke Hirano and Guido W Imbens. The propensity score with continuous treatments. *Applied Bayesian modeling and causal inference from incomplete-data perspectives*, 226164:73–84, 2004.
- Brantly Callaway, Andrew Goodman-Bacon, and Pedro HC Sant’Anna. Difference-in-differences with a continuous treatment. *arXiv preprint arXiv:2107.02637*, 2021.
- Patrick Schwab, Lorenz Linhardt, Stefan Bauer, Joachim M Buhmann, and Walter Karlen. Learning counterfactual representations for estimating individual dose-response curves. In *Proceedings of the AAAI Conference on Artificial Intelligence*, volume 34, pages 5612–5619, 2020.
- Iván Díaz and Mark J van der Laan. Targeted data adaptive estimation of the causal dose–response curve. *Journal of Causal Inference*, 1(2):171–192, 2013.
- Mark J Van der Laan and Sherri Rose. *Targeted learning in data science*. Springer, 2018.
- Edward H Kennedy, Zongming Ma, Matthew D McHugh, and Dylan S Small. Non-parametric methods for doubly robust estimation of continuous treatment effects. *Journal of the Royal Statistical Society Series B: Statistical Methodology*, 79(4):1229–1245, 2017.
- Jerome Friedman, Trevor Hastie, Rob Tibshirani, Balasubramanian Narasimhan, Kenneth Tay, Noah Simon, and Junyang Qian. Package ‘glmnet’. *CRAN R Repository*, 595, 2021.

A Data Generating Distributions (DGDs)

Table 3: List of Underling Data Generating Distributions (DGDs)

Simulation	DGD
1	<ul style="list-style-type: none"> • Exogenous variables: <ul style="list-style-type: none"> - $U_W \sim Normal(\mu = 0, \sigma^2 = 1^2)$ - $U_A \sim Normal(\mu = 0, \sigma^2 = 2^2)$ - $U_Y \sim Uniform(min = 0, max = 1)$ • Structural equations F and endogenous variables: <ul style="list-style-type: none"> - $W = U_W$ - $A = bound(2 - 0.5W + U_A, min = 0, max = 5)$ - $Y = \mathbf{I}[U_Y < expit(-3 + 0.5W + 1.25A - 0.5WA)]$
2	<ul style="list-style-type: none"> • Exogenous variables: <ul style="list-style-type: none"> - $U_W \sim Normal(\mu = 0, \sigma^2 = 1^2)$ - $U_A \sim Normal(\mu = 0, \sigma^2 = 1.3^2)$ - $U_Y \sim Uniform(min = 0, max = 1)$ • Structural equations F and endogenous variables: <ul style="list-style-type: none"> - $W = U_W$ - $A = bound(2.5 - 0.5W + U_A, min = 0, max = 5)$ - $Y = \mathbf{I}[U_Y < expit(-5 + 3W + 5sin(1.25A^{1.5}) + 3WA)]$
3	<ul style="list-style-type: none"> • Exogenous variables: <ul style="list-style-type: none"> - $U_W \sim Normal(\mu = 0, \sigma^2 = 1^2)$ - $U_A \sim Normal(\mu = 0, \sigma^2 = 2^2)$ - $U_Y \sim Uniform(min = 0, max = 1)$ • Structural equations F and endogenous variables: <ul style="list-style-type: none"> - $W = U_W$ - $A = bound(2 - 0.5W + U_A, min = 0, max = 5)$ - $Y = \mathbf{I}[U_Y < expit(-4 - 2W + 1.5A + \mathbf{I}(A > 2)1.5sin((0.8A)^2 - 2.56))]$
4	<ul style="list-style-type: none"> • Exogenous variables: <ul style="list-style-type: none"> - $U_W \sim Normal(\mu = 0, \sigma^2 = 1^2)$ - $U_A \sim Normal(\mu = 0, \sigma^2 = 1^2)$ - $U_Y \sim Uniform(min = 0, max = 1)$ • Structural equations F and endogenous variables: <ul style="list-style-type: none"> - $W = U_W$ - $A = bound(2.5 - 0.5W + U_A, min = 0, max = 5)$ - $Y = \mathbf{I}[U_Y < expit(-2 + W + \mathbf{AI}(A \geq 2) - \mathbf{AI}(A \geq 4) - 0.5WA)]$